Available online at www.sciencedirect.com
SCIENCE DIRECT®
PERGAMON
International Journal of Heat and Mass Transfer 46 (2003) 3789–3796
International Journal of HEAT and MASS TRANSFER
www.elsevier.com/locate/ijhmt

Prediction of the frost formation on a cold flat surface

Kwan-Soo Lee [a,*], Sung Jhee [b], Dong-Keun Yang [a]

[a] School of Mechanical Engineering, Hanyang University, 17 Haengdang-dong, Sungdong-gu, Seoul 133-791, South Korea
[b] Digital Appliance Research Laboratory, LG Electronics Inc., 327-23 Gasan-dong, Keumchun-gu, Seoul 153-802, South Korea

Received 6 September 2002; received in revised form 4 April 2003

Abstract

A mathematical model is presented to predict the behavior of frost formation by simultaneously considering the air flow and the frost layer. The present model is validated by comparing with several other analytical models and our experiments. It is found that most of the previous models cause considerable errors depending on the working conditions or the correlations used in predicting the frost thickness growth, whereas the model in this work estimates the thickness, density, and surface temperature of the frost layer more accurately within an error of 10% except the early stage of frosting in comparison with the experimental data. Numerical results are presented for the variations of heat and mass transfer during the frost formation and for the behavior of frost layer growth along the direction of air flow. Also, a correlation between the convective heat and mass transfer is obtained as $Le^{(1-n)} = 0.905 \pm 0.005$ in this work.

1. Introduction

Frost layer formed on the surface of a heat exchanger acts as a thermal barrier and contributes to flow resistance, thus degrading the performance of the heat exchanger. Therefore, it is very important in designing a heat exchanger to accurately predict the behavior of the frost layer growth and the accompanying heat and mass transfer.

It has been reported that the frosting process exhibits different features for each characteristic growth period [1]. It has been also shown that the frost layer properties and the surface temperature vary with time and location during the frosting. However, most of the frosting time is occupied by the frost layer growth period over which the frost layer grows uniformly. Thus, the behavior of frost layer growth can be approximately predicted by modeling the frost layer with appropriate simplifying assumptions.

Most existing models to analyze the frost formation can be classified into two categories. The first is the one which predicts the variations of frost properties from the diffusion equation applied to the frost layer and then calculates the amount of heat and mass transfer in the frost layer by using the correlations on the air-side without solving the outside region of the frost layer [2–5]. Recently, different approaches [6–10] that treat the frost layer as a porous medium have been attempted. However, there are several unknown coefficients to be determined for the mass diffusion. The second modeling method analyzes the air flow with boundary layer equations and predicts the frost properties by using the correlations [11,12]. In this method, one should select the appropriate correlations, and the accuracy of the numerical result is dependent on the choice of these correlations. Also, in these models, only the frost thickness is predicted without giving any information on the density or the surface temperature of the frost layer.

Therefore, the objective of this study is to develop a mathematical model for predicting the behavior of frost layer growth without employing experimental correlations. This model includes partial differential equations for the boundary layer to consider the variation of air flow during frost formation and a modified diffusion equation for the frost layer to predict the frost properties. The present study provides the additional numerical results on the characteristics of the heat and mass transfer under frosting.

* Corresponding author. Tel.: +82-2-2290-0426; fax: +82-2-2295-9021.
E-mail address: ksleehy@hanyang.ac.kr (K.-S. Lee).

0017-9310/03/$ - see front matter © 2003 Elsevier Ltd. All rights reserved.
doi:10.1016/S0017-9310(03)00195-9

Nomenclature

c_p	specific heat at constant pressure [kJ/kg K]
D	diffusivity [m^2/s]
g	acceleration of gravity [m/s^2]
h_h	heat transfer coefficient [W/m^2 K]
h_m	mass transfer coefficient [kg/m^2 s]
h_{sv}	latent heat of sublimation [kJ/kg]
k	thermal conductivity [W/m K]
L	length of cooling plate [m]
Le	Lewis number
m''	mass flux [kg/m^2 s]
m''_y	mass flux for frost thickness [kg/m^2 s]
m''_ρ	mass flux for frost density [kg/m^2 s]
m_w	mass concentration of vapor
p	pressure [Pa]
q''	heat flux [W/m^2]
T	temperature [°C]
t	time [min]
u, v	velocity components [m/s]
y_f	frost layer thickness [m]

Greek symbols

α	thermal diffusivity of air [m^2/s]
α_f	absorption factor [s^{-1}]
δ_{ij}	Kronecker delta function
μ	viscosity [kg/m s]
ρ	density [kg/m^3]
ω	absolute humidity [kg/kg$_a$]

Subscripts

a	air side
eff	effective value
f	frost
fs	frost surface
i, j	tensor indexes
in	inlet
init	initial
p	cooling plate
sat	saturation
x	local
w	water vapor
∞	free stream condition

2. Physical model and formulation

The present work analyzes the behavior of frost layer growth which occurs between the cold flat plate, maintained at T_p below the freezing temperature, and the humid air flowing at a constant velocity of u_{in}. Numerical analysis is performed to predict the frost layer growth and the characteristics of the heat and mass transfer in the configuration of Fig. 1.

In order to predict the behavior of frost layer growth, it is assumed that all processes are quasi-steady state and the variation of frost density in the direction normal to the cooling plate is negligible. The governing equations for the air-side and the frost layer then can be given as follows.

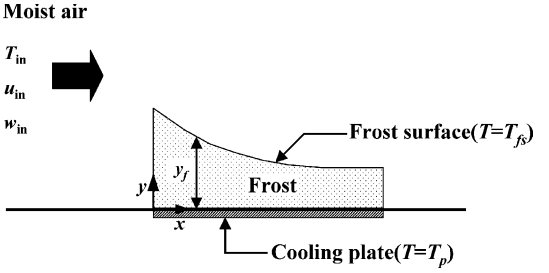

Fig. 1. Schematic diagram of the frost formation on a cold flat surface.

2.1. Air-side governing equations

The governing equations consist of continuity, momentum, energy, and mass concentration equations. Assuming incompressible laminar flow with no viscous dissipation and taking the Boussinesq approximation, the equations in tensor form can be expressed as follows:

$$\frac{\partial u_i}{\partial x_i} = 0 \tag{1}$$

$$\rho \frac{\partial}{\partial x_j}(u_i u_j) = -\frac{\partial p}{\partial x_i} + \frac{\partial}{\partial x_j}\left(\mu \frac{\partial u_i}{\partial x_j}\right) + g(\rho_\infty - \rho)\delta_{i2} \tag{2}$$

$$\rho c_p \frac{\partial}{\partial x_j}(T u_j) = \frac{\partial}{\partial x_j}\left(k_a \frac{\partial T}{\partial x_j}\right) \tag{3}$$

$$\rho \frac{\partial}{\partial x_j}(m_w u_j) = \frac{\partial}{\partial x_j}\left(\rho D \frac{\partial m_w}{\partial x_j}\right) \tag{4}$$

2.2. Frost layer governing equations

The governing equations in the porous frost layer are composed of a modified diffusion equation for predicting the frost layer growth and an energy equation for evaluating the heat transfer inside the layer. It is assumed that the amount of water vapor absorbed into a control volume is proportional to the water vapor density in the control volume [5]. Then the diffusion equation could be modified as

$$D\frac{d^2\rho_w}{dy^2} = \alpha_f \rho_w \tag{5}$$

where D represents the diffusivity of the water vapor in the air [13], and α_f indicates an absorption factor [5].

Heat transfer within the frost layer can be analyzed by introducing the effective thermal conductivity of the frost layer.

$$\rho c_p \frac{\partial}{\partial x_j}(Tu_j) = \frac{\partial}{\partial x_j}\left(k_{f,eff}\frac{\partial T}{\partial x_j}\right) \tag{6}$$

The effective thermal conductivity of the frost layer is known to be closely related to the frost density. In this study, the following correlation proposed by Lee et al. [14] is used:

$$k_{f,eff} = 0.132 + 3.13\times10^{-4}\rho_f + 1.6\times10^{-7}\rho_f^2 \tag{7}$$

2.3. Initial and boundary conditions

The appropriate initial and boundary conditions, with reference to Fig. 1, are as follows.

2.3.1. Frost layer initial conditions

For the computation of frost layer growth, it is required to provide the frost layer thickness and density at an early stage of frost formation. These initial values should be taken considering not only the effects of the working conditions but also those of the surface characteristics on the frost properties. To avoid numerical arbitrariness, the proper values are to be provided from the experimental data.

$$\rho_f = \rho_{f,init}, \quad y_f = y_{f,init} \tag{8}$$

2.3.2. Boundary conditions

Inlet/outlet of air flow. Working conditions of the air flow are taken as the inlet condition. Boundary conditions at the outlet are taken as zero gradients because the length of duct is so long that it rarely affects the upstream flow field.

$$\text{Inlet}: \quad u = u_{in}, \quad v = 0, \quad T = T_{in}, \quad m_w = m_{w,in} \tag{9}$$

$$\text{Outlet}: \quad \frac{\partial u}{\partial x} = 0, \quad \frac{\partial v}{\partial x} = 0, \quad \frac{\partial T}{\partial x} = 0, \quad \frac{\partial m_w}{\partial x} = 0 \tag{10}$$

Duct surfaces. No-slip and adiabatic conditions are imposed on the impermeable duct surfaces.

$$u = 0, \quad v = 0, \qquad \frac{\partial T}{\partial y} = 0, \quad \frac{\partial m_w}{\partial y} = 0 \tag{11}$$

Cooling plate surface. The surface temperature of the cooling plate is maintained constant at T_p, and the water vapor is assumed to be saturated. The gradient of the mass concentration of water vapor on the impermeable surface is set to zero.

$$T = T_p, \quad m_w = m_{w,sat}(T_p), \quad \frac{\partial m_w}{\partial y} = 0 \tag{12}$$

Interface (frost layer surface). No-slip condition is imposed on the frost layer surface. The normal velocity at the surface due to vapor diffusion is assumed to be zero since it has negligible effect on the transport process [12]. The water vapor on the surface is assumed to be saturated.

$$u = 0, \quad v = 0, \quad m_w = m_{w,sat}(T_{fs}) \tag{13}$$

As a matching condition for the coupled governing equations, the energy balance between the air flow and the frost layer should be satisfied as follows:

$$k_{f,eff}\left(\frac{\partial T}{\partial y}\right)_{y=y_f^-} = k_a\left(\frac{\partial T}{\partial y}\right)_{y=y_f^+} + \rho h_{sv} D\left(\frac{\partial m_w}{\partial y}\right)_{y=y_f^+} \tag{14}$$

2.4. Calculation of frost properties

The water vapor transferred into the frost surface from moist air increases both the frost density and thickness. This phenomenon can be expressed as follows:

$$m_f'' = \rho D\frac{\partial m_w}{\partial y}\bigg|_{y_f} = m_y'' + m_\rho'' \tag{15}$$

The mass flux for the frost density absorbed into frost layer is given by

$$m_\rho'' = \int_{y=0}^{y=y_f} \alpha_f \rho_w \, dy \tag{16}$$

The frost density and thickness for each time interval are calculated as follows [3]:

$$\rho_f^{t+\Delta t} = \rho_f^t + \frac{m_\rho''}{y_f}\Delta t$$
$$y_f^{t+\Delta t} = y_f^t + \frac{m_y''}{\rho_f}\Delta t \tag{17}$$

3. Numerical scheme

Numerical computations to predict the frost layer growth can be summarized as follows:

(i) Given a frost layer surface temperature, the corresponding mass concentration of saturated water vapor on the surface is calculated.

(ii) By solving the governing equations for the air side and the frost layer, the amount of heat and mass transfer on the frost layer surface is obtained.
(iii) Procedures (i) and (ii) are repeated until Eq. (14) is satisfied.
(iv) With the frost surface temperature, the frost layer thickness and the density at the present time step are determined.
(v) Procedures (i)–(iv) are repeated until it reaches the desired time.

The governing equations are discretized by using the finite-volume scheme and are calculated iteratively by employing the SIMPLER algorithm, wherein the control volumes for the temperature and pressure are staggered from those for the velocities [15]. The computations are performed on the grids of non-uniform mesh which are densely packed above the frost layer surface. The grid dependence test is performed by changing the number of grid points. The grid system used in the present model is 46×55 by considering that the changes of frost properties are less than 1%. The effects of the time step on the numerical results are examined for four time steps: 6, 10, 12, and 30 s. It is found that the numerical results on the frost properties do not change significantly when the time step is less than 10 s. Thus, all the numerical results presented in this paper are calculated with a time step of 10 s. The computation results are assumed to be converged if the change of frost surface temperature, calculated from the matching condition given by Eq. (14) in successive iterations, is less than 0.0005%.

4. Experiment

Fig. 2 shows the experimental apparatus used in this study. The apparatus is composed of four sections: the climate chamber controlling the humidity and temperature of the inlet air, the cooling section maintaining the surface temperature of the cooling plate, the test section (length of 300 mm, width of 150 mm and height of 150 mm) measuring and observing the frost layer, and the circulation section controlled by the blower with an inverter. Each section of the apparatus is controlled individually [16].

The flow rate and temperature of the refrigerant circulated in the cooling section are controlled by a pump and refrigerator, respectively. A solution of ethyleneglycol and distilled water mixed at a ratio of 6:4 is used as the refrigerant. The temperature and humidity of the inlet/outlet air in the test section are measured by type-T thermocouples and humidity sensors, respectively. Also, the flow rate of the air flow is measured by using the flow nozzle.

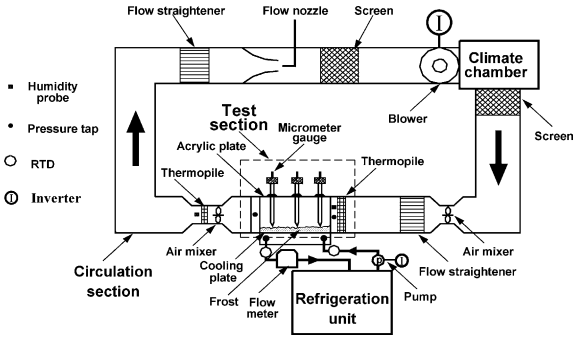

Fig. 2. Schematic of experimental apparatus.

Table 1
Uncertainities of parameters

Parameter	Uncertainty (%)
Frost surface temperature	4.36
Frost thickness	5.57
Frost density	6.94
Total heat flux	3.69

Before starting frosting experiment, the surface of the cooling plate is cleared and the aluminum tapes are attached on the surface of the cooling plate for the measurement of frost mass. To prevent the frost formation on the cooling plate before reaching experimental condition, vinyl wrap is attached on the surface of the cooling plate. The climate chamber and the cooling section are operated to control the experimental condition. After the experimental condition reaches the steady state, the frosting experiment is started by removing the vinyl wrap.

The thickness and surface temperature of frost layer are measured by using a digital micrometer and an infrared thermometer, respectively. Also, the aluminum tapes attached on the surface of the cooling plate are detached to weigh the frost mass by using a chemical balance, and then frost density is calculated by the frost thickness and frost mass at 0.25, 0.5, 1.0, 1.5, 2.0, 2.5 and 3.0 h.

Table 1 presents the uncertainties of the measured data calculated by considering the bias error and the accuracy of the measuring devices [17]. The uncertainties are calculated based on the data obtained from the experimental conditions as follows: inlet air temperature of 15 °C, absolute humidity of 0.00633 kg/kg_a, air velocity of 2.5 m/s and surface temperature of the cooling plate of −15 °C.

5. Results and discussion

The results of the present model are compared with those of various existing models [2,4,11] and the exper-

iment to verify its validity. The numerical results on the heat and mass transfer inside the frost layer, which are difficult to obtain from experiments, are also presented.

Fig. 3 shows the experimental data of Jones and Parker [2] and the numerical predictions using the various models [2,4,11], including the present model. Among the existing models which use the correlations on the frost properties or the heat and mass transfer, Sami and Duong's model [4] predicts the thickness relatively well in the case of low humidity. However, it overpredicts in the case of high humidity ($\omega = 0.0150$ kg/kg$_a$). Sherif et al.'s model [11] shows little effect of absolute humidity on the frosting rate, and Jones and Parker's model [2] underpredicts the frost growth. These models show the error of 10–30% in the frost thickness growth, whereas the present model predicts the frost growth within an error of 10%.

In Figs. 4–6, the numerical results of the present model are compared with the experimental data to validate the present model. Fig. 4 presents a comparison of the numerical results with the present experimental data on the frost layer thickness. It is shown that the present model predicts the growth of frost layer thickness within an error of 10%. The frost layer grows rapidly at the early stage, and then its growth rate gradually slows down. It is revealed that the frost layer growth is accelerated with higher inlet velocity and absolute humidity.

Fig. 5 compares the numerical results on the frost density with the present experimental data. It is shown that there exists a relatively large error during the first 15 min between the present numerical results and the experimental data. After that period, the present model predicts the density within an error of 10%. The large error at the early stage may be attributed to the experimental uncertainties which stem from the measurement of the minute weight of the frost at that stage. The frost density increases rapidly at the beginning, but the increment is small after $t = 90$ min.

Fig. 6 presents a comparison between the numerical results and experimental data on the frost layer surface temperature. There are few experimental data available since it is very difficult to measure the frost surface temperature within a reasonable error. The present model predicts the variation of the frost surface temperature correctly. The surface temperature increases rapidly at the early stage when the frost layer grows fast, but the increase rate is reduced as its growth rate decreases.

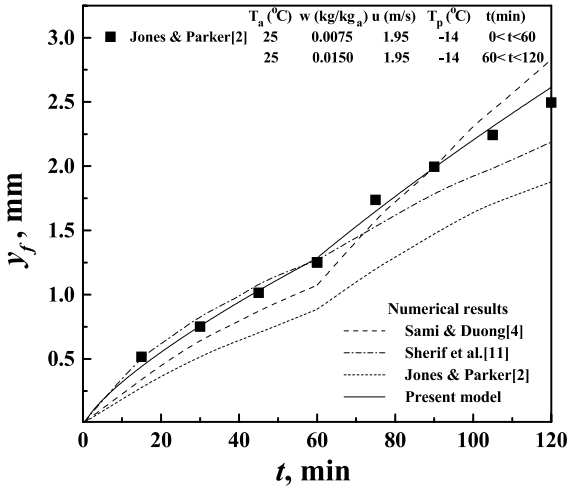

Fig. 3. Comparison of the frost layer thickness for various numerical models.

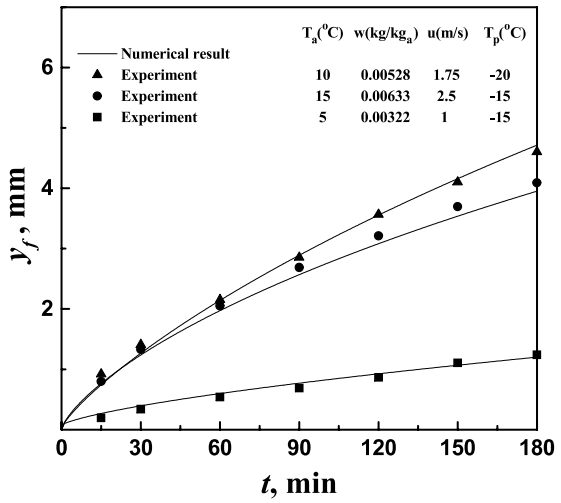

Fig. 4. Comparison of the present numerical results with experimental data on the frost layer thickness.

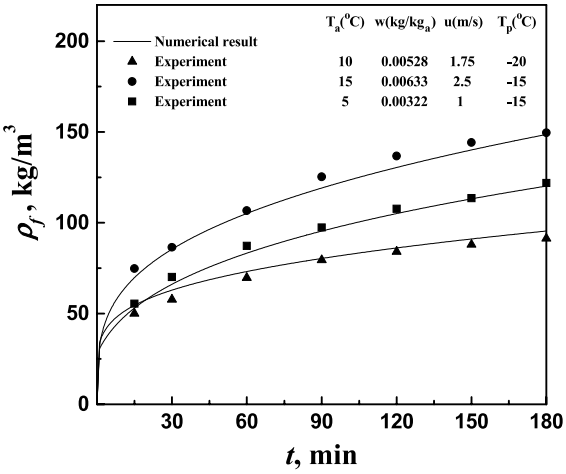

Fig. 5. Comparison of the present numerical results with experimental data on the frost density.

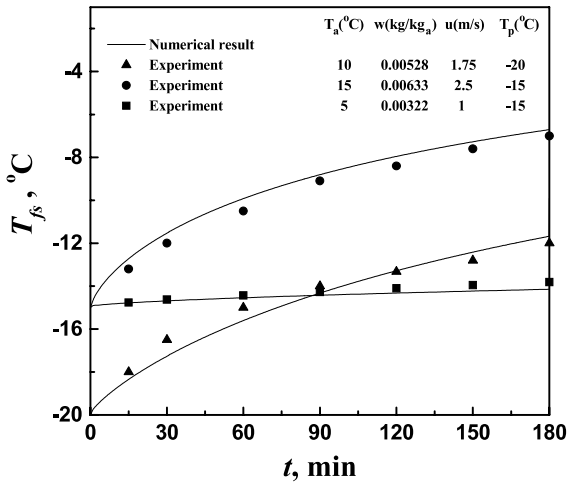

Fig. 6. Comparison of the present numerical results with experimental data on the frost surface temperature.

The behavior of the frost layer growth includes not only the variation of the frost properties but also the characteristics of the overall heat and mass transfer. Thus, it is required to analyze the heat and mass transfer to more accurately predict the frost layer growth. Fig. 7 shows the variation of heat flux during the frost formation. The heat flux after 180 min of operation is reduced by 25%, compared to that at the beginning of frosting. The sensible heat transfer rate decreases continuously during the frosting as the surface temperature of the frost layer increases with its growth. However, the latent heat transfer rate maintains an almost constant value after a slight drop at the beginning. Consequently, the variation of the total heat flux resembles the curve of the sensible heat flux. This may be due to the fact that the potential of mass transfer remains almost constant because the saturated absolute humidity on the frost surface is not changed very much with the increase of its temperature. It is found that there are good agreements between the numerical results and the experimental data.

Fig. 8 presents the numerical results on the variation of the mass flux during the frosting. The variation of the mass flux shows a similar trend to that of the heat flux. About 70% of the mass flux is responsible for the increase of the frost thickness. This result is different from White and Cremers's assumption [18] that the densification of frost is due to half the mass being transferred to the frost layer. This is due to the fact that the growth of frost layer properties strongly depends on the operating conditions. Despite the fact that the total mass flux decreases with the frost growth, the mass flux for the densification increases slightly. This results from the fact that the humidity difference between the cooling plate and frost layer surface increases as the frost surface temperature rises with frost layer growth.

Fig. 9 depicts the variations of frost properties with respect to the distance from the inlet at $t = 180$ min. At the inlet, the heat and mass transfer occurs actively by the leading edge effect so that the thickness and density of the frost layer have the largest values. As the humid air flows along a cold plate, the temperature and the humidity of the air decrease due to the upstream heat and mass transfer with cold surface. Thus, the thickness and the density of the frost layer decrease with distance from the leading edge.

Fig. 10 shows the correlation of the heat and mass transfer coefficients during the frosting. The analogy between convective heat and mass transfers can be expressed as follows:

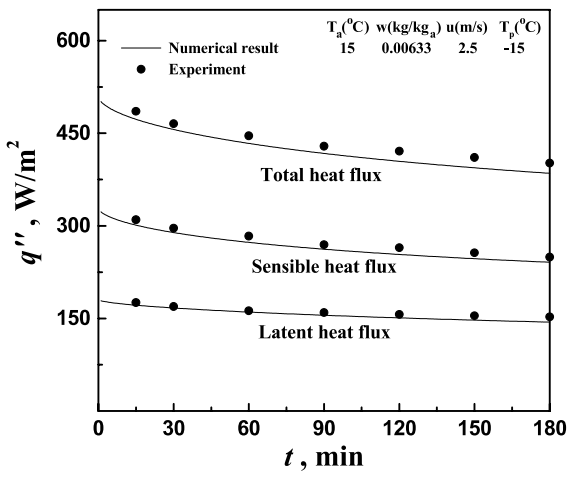

Fig. 7. Temporal variation of heat flux.

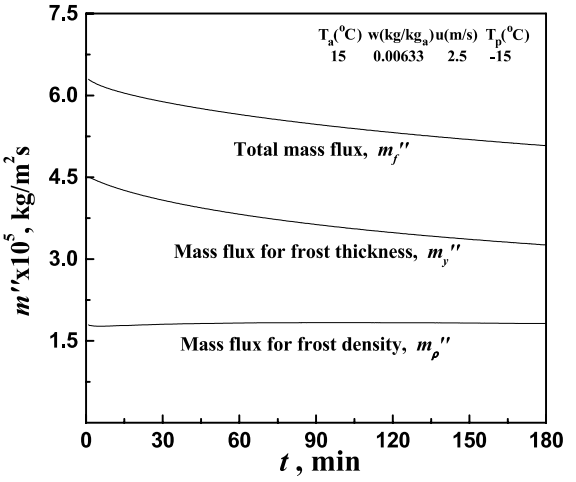

Fig. 8. Temporal variation of mass flux.

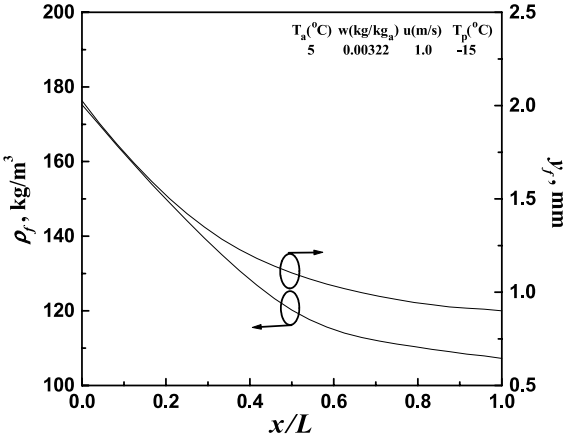

Fig. 9. Variations of the frost properties along the distance from the inlet at $t = 180$ min.

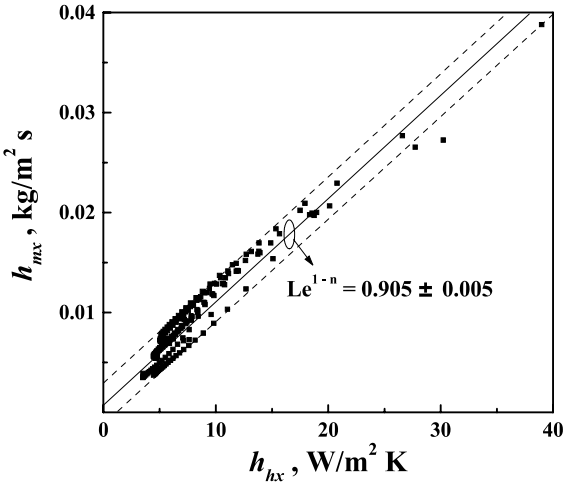

Fig. 10. Correlation between the heat and the mass transfer coefficients.

$$\frac{h_{\mathrm{h}}}{h_{\mathrm{m}}} = c_p\left(\frac{\alpha}{D}\right)^{(1-n)} = c_p Le^{(1-n)} \tag{18}$$

Many researchers [2–8,11] assumed that the Lewis number is equal to unity for the calculation of the mass transfer coefficient for convenience of analysis. However, the correlation obtained from the present numerical results is given as

$$Le^{(1-n)} = 0.905 \pm 0.005 \tag{19}$$

Therefore, it is believed that the previous works obtained from the model using the assumption of "$Le = 1$" may lead to yield more error, compared with those of the present model.

6. Conclusions

This study presents a mathematical model to predict the frost layer growth and the characteristics of its heat and mass transfer by coupling the air flow with the frost layer. The model is validated by comparing the present numerical results with those of both analytical and experimental data. The previous models cause considerable error depending on the working conditions or correlations used in the prediction of the frost thickness growth. However, the present model predicts the behavior of frost formation accurately within an error of 10% except the early stage of frosting, compared with experimental data. The heat transfer rate decreases rapidly at the early stage of frosting, but the rate of decrement is reduced gradually with time. On the other hand, the latent heat transfer rate, contrary to the sensible heat transfer rate, maintains an almost constant value. The variation of mass transfer rate shows a similar trend to that of the heat transfer rate, and the relative magnitude of the frost thickness growth and the densification varies as the frost layer grows. The thickness and density of the frost layer have the largest values at the inlet owing to the leading edge effect, and decrease with distance from the leading edge. Caution has to be taken when the assumption of "$Le = 1$" is used.

Acknowledgements

This research was supported by The Center of Innovative Design Optimization Technology (iDOT), Korea Science and Engineering Foundation.

References

[1] Y. Hayashi, A. Aoki, S. Adachi, K. Hori, Study of frost properties correlating with frost formation types, J. Heat Transfer 99 (1977) 239–245.
[2] B.W. Jones, J.D. Parker, Frost formation with varying environmental parameters, J. Heat Transfer 97 (1975) 255–259.
[3] A.Z. Sahin, An analytical study of frost nucleation and growth during the crystal growth period, Heat Mass Transfer 30 (1995) 321–330.
[4] S.M. Sami, T. Duong, Mass and heat transfer during frost growth, ASHRAE Trans. 95 (1) (1989) 158–165, No. 3218.
[5] K.S. Lee, W.S. Kim, T.H. Lee, A one-dimensional model for frost formation on a cold flat surface, Int. J. Heat Mass Transfer 40 (18) (1997) 4359–4365.
[6] R. Le Gall, J.M. Grillot, C. Jallut, Modelling of frost growth and densification, Int. J. Heat Mass Transfer 40 (13) (1997) 3177–3187.
[7] K.A.R. Ismail, C.S. Salinas, Modeling of frost formation over parallel cold plates, Int. J. Refrig. 22 (5) (1999) 425–441.

[8] T.-X. Tao, R.W. Besant, K.S. Rezkallah, A mathematical model for predicting the densification and growth of frost on a flat plate, Int. J. Heat Mass Transfer 36 (1993) 353–363.
[9] Y. Mao, R.W. Besant, H. Chen, Frost characteristics and heat transfer on a flat plate under freezer operating conditions: Part II. Numerical modeling and comparison with data, ASHRAE Trans. 105 (1) (1999) 252–259.
[10] A. Lüer, H. Beer, Frost deposition in a parallel plate channel under laminar flow conditions, Int. J. Therm. Sci. 39 (2000) 85–95.
[11] S.A. Sherif, S.P. Raju, M.M. Padki, A.B. Chan, A semi-empirical transient method for modeling frost formation on a flat plate, ASME Heat Transfer Div. 139 (1990) 15–23.
[12] H.C. Parish, C.F. Sepsy, A numerical analysis of frost formation under forced convection, ASHRAE Semiannual Meeting, New Orleans, LA., Paper no. 2331, 1972, pp. 236–251.
[13] ASHRAE Handbook, 1993, Fundamentals, 6.15.
[14] K.S. Lee, T.H. Lee, W.S. Kim, Heat and mass transfer of parallel plate heat exchanger under frosting condition, Kor. J. Air-Cond. Refrig. Eng. 6 (2) (1994) 155–165.
[15] S.V. Patankar, Numerical Heat Transfer and Fluid Flow, Hemisphere/McGraw-Hill, Washington, DC, 1980.
[16] K.S. Lee, W.S. Kim, The effects of design and operating factors on the frost growth and thermal performance of a flat plate fin-tube heat exchanger under the frosting condition, KSME Int. J. 13 (12) (1999) 973–981.
[17] S.J. Kline, F.A. McClintock, Describing uncertainties in single-sample experiments, Mech. Eng. 75 (1953) 3–8.
[18] J.E. White, C.J. Cremers, Prediction of growth parameters of frost deposits in forced convection, J. Heat Transfer 103 (1981) 3–6.